Available online at www.sciencedirect.com
ScienceDirect
Trans. Nonferrous Met. Soc. China 30(2020) 2326−2338
Transactions of Nonferrous Metals Society of China
www.tnmsc.cn

Microstructure and mechanical properties of squeeze-cast Al−5.0Mg−3.0Zn−1.0Cu alloys in solution-treated and aged conditions

Tian-wen LIU, Qu-dong WANG, Hua-ping TANG, Zhong-yang LI, Chuan LEI, Mahmoud EBRAHIMI, Hai-yan JIANG, Wen-Jiang DING

National Engineering Research Center of Light Alloy Net Forming and Key State Laboratory of Metal Matrix Composites, School of Materials Science and Engineering, Shanghai Jiao Tong University, Shanghai 200240, China

Received 30 December 2019; accepted 11 July 2020

Abstract: The microstructure and mechanical properties at different depths of squeeze-cast, solution-treated and aged Al−5.0Mg−3.0Zn−1.0Cu alloy were investigated. For squeeze-cast alloy, from casting surface to interior, the grain size of α(Al) matrix and width of T-$Mg_{32}(AlZnCu)_{49}$ phase increase significantly, while the volume fraction of T phase decreases. The related mechanical properties including ultimate tensile strength (UTS) and elongation decrease from 243.7 MPa and 2.3% to 217.9 MPa and 1.4%, respectively. After solution treatment at 470 °C for 36 h, T phase is dissolved into matrix, and the grain size increases so that the UTS and elongation from surface to interior are respectively reduced from 387.8 MPa and 18.6% to 348.9 MPa and 13.9%. After further peak-aging at 120 °C for 24 h, numerous G.P. II zone and η' phase precipitate in matrix. Consequently, UTS values of the surface and interior increase to 449.5 and 421.4 MPa, while elongation values decrease to 12.5% and 8.1%, respectively.
Key words: squeeze-cast Al−Zn−Mg−Cu alloys; solution treatment; aging; microstructures; mechanical properties

1 Introduction

In recent years, Al−Zn−Mg−Cu alloys have drawn increasing attention due to their remarkable advantages such as light weight, high strength, and suitable ductility [1−3]. Compared with Al−Zn−Mg−Cu wrought alloys by various deformation processes, Al−Zn−Mg−Cu cast alloys present an economically alternative way, especially in the automotive industry. Previous studies [4−9] have pointed out that the Al−Zn−Mg−Cu alloys prepared by the gravity casting exhibit high tensile strength, exceeding 450 MPa. However, the ductility of the mentioned alloys is poor (only about 2%) due to the coarse microstructure, micro-pores, and shrinkage defects forming during the solidification [10,11]. To overcome these obstacles, squeeze-casting which is considered as a promising casting process has been widely applied in Al−Zn−Mg−Cu alloys since the imposed high pressure during the process refines the microstructure and feeds the solidification shrinkage [12−14]. HASHEMI et al [15] reported that the squeeze-cast Al−(7.5−8)Zn−(2.5−3)Mg−(1.4−1.6)Cu alloy led to a good combination of strength (500 MPa) and ductility (10%). CHADWICK and YUE [16,17] also stated that the mechanical properties of squeeze-cast 7010 alloys are comparable to those of 7010 wrought alloys.

For squeeze-cast Al−Zn−Mg−Cu alloys, different imposed pressures and cooling rates between the casting surface and interior zones lead to various microstructures which consequently change the mechanical properties [18]. It was stated by TANG et al [19] that the α(Al) grain size and eutectic morphologies are mainly dependent on the

Foundation item: Projects (51674166, U1902220) supported by the National Natural Science Foundation of China
Corresponding author: Qu-dong WANG; Tel: +86-21-54742715; E-mail: wangqudong@sjtu.edu.cn
DOI: 10.1016/S1003-6326(20)65382-1

casting parameters such as pouring speed and cooling rate. For Al−Zn−Mg−Cu cast alloys, different microstructures between the surface and the central region may due to the different distributions of alloying elements after the solution treatment. The elemental distributions can affect precipitation behavior and related mechanical properties during aging. POURKI et al [20] demonstrated that a higher cooling rate improves the strength of Al−12.0Zn− 3.0Mg−2.5Cu cast alloy under the T6 condition. Overall, the heterogeneous microstructure leads to different mechanical properties from the casting surface to the interior of the squeeze-cast Al−Zn−Mg−Cu alloys. However, the study of such complex mechanical properties of squeeze-cast Al−Zn−Mg−Cu alloys under different heat-treated conditions is still lacking and needs further investigations.

In this research, Al−5.0Mg−3.0Zn−1.0Cu alloy was produced by indirect squeeze casting and subjected to different heat treatments. Then, microstructure and mechanical properties of the casting surface and central region under the squeeze-cast, solution-treated, and aged conditions were comprehensively investigated.

2 Experimental

The studied alloy was prepared using pure Al (99.7%), pure Mg (99.8%), pure Zn (99.7%), and Al−50%Cu master alloy (all compositions in this work was in wt.% unless otherwise stated) melted into a graphite crucible in an electric resistance furnace at 720 °C. The melt was degassed with 0.2% C_2Cl_6. As the melting temperature reached 660 °C, it was poured into the squeeze-casting die which was preheated up to 200 °C. The imposed pressure was 125 MPa during the process. Eventually, the specimen was about 160 mm in height and 80 mm in thickness. The chemical composition of the alloy was determined by inductively coupled plasma-atomic emission spectrometry (ICP-AES) and listed in Table 1.

The specimens were then solution-treated at 470 °C for different time ranging from 1 to 36 h and subsequently quenched into water of 25 °C. Afterward, the solution-treated (470 °C, 36 h) alloy was aged at 120 °C for various time from 0 to 48 h in the electric oil bath furnace.

Table 1 Chemical composition of Al−5.0Mg−3.0Zn−1.0Cu alloy (wt.%)

Mg	Zn	Cu	Fe	Si	Al
4.87	3.03	0.93	0.07	0.03	Bal.

Specimens for microstructural observation and quantitative analysis were taken from both the surface and interior zones (depth of 0, 2.0 and 4.0 mm) of the casting, as shown in Fig. 1(a). The constituent phases were identified by a poly-functional X-ray diffractometer (XRD) with a Cu K_α source operating at 25 kV, 50 mA, and a scanning rate of 5 (°)/min. It should be mentioned that these specimens were etched by Keller etchant for 10 s to prepare the metallographic samples. The microstructures were characterized through Zeiss-Axio Observer A1 polarized optical microscope (OM). The polished samples were analyzed by scanning electron microscopy (SEM, Phenom XL) equipped with an energy dispersive spectroscopy (EDS). Also, the size and volume fraction of primary α(Al) and secondary phases of the cast alloy under different conditions were measured by Image-Pro Plus software. Furthermore, a FEI-Tecnai G2 TF20 transmission electron microscopy (TEM) operating at 200 kV was used for the morphological observation of precipitates. According to Fig. 1(b), the TEM samples were cut from the end of the tensile specimen.

Vickers hardness (HV) measurements were performed to investigate age-hardening behavior at a load of 0.5 kg for dwell time of 10 s. The average

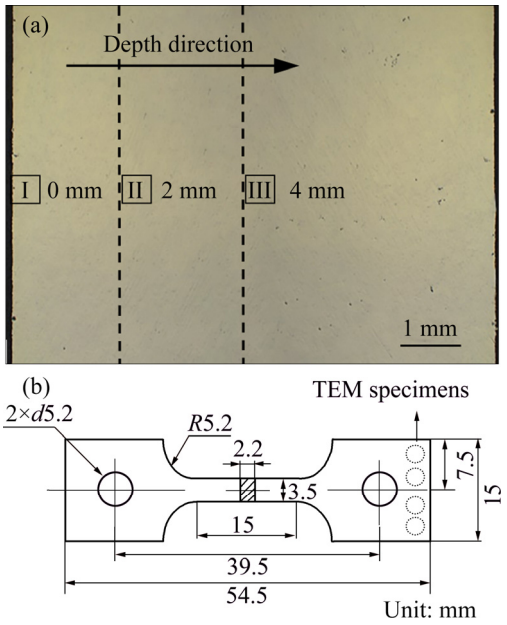

Fig. 1 Schematic of different observed positions (a) and tensile specimens (b)

of eight hardness measurements was reported for each condition. Tensile samples were sliced from the casting surface and interior (depth of 0, 2.0 and 4.0 mm) and the dimension of tensile sample was represented in Fig. 1(b). Tensile tests were carried out at room temperature using Zwick/Roell Z020 tensile machine at a strain rate of 1.6×10^{-4} s^{-1}. Three tensile tests were performed for each condition and the average value was taken as the tensile result. Afterward, the fracture surface was analyzed through the SEM.

3 Results and discussion

3.1 Microstructure and mechanical properties of squeeze-cast alloy

Figure 2 represents the microstructure in three different regions, as marked in Fig. 1(a). Accordingly, equiaxed α(Al) grains and different strip-like intermetallics are observed. As shown in Figs. 2(a−d), the microstructures remain unchanged between the surface and the depth of 2.0 mm which are composed of α(Al) grains and secondary phases. It should be mentioned that the α(Al) grains with both equiaxed and dendritic characteristics are recognizable. As shown in Figs. 2(e, f), a noticeable change of the microstructure is observed at the depth of 4.0 mm as compared to the surface. Both of the α(Al) grains and the secondary phases become coarser and the primary α(Al) grains have the equiaxed shape due to the decrease of the cooling rate, which is in good agreement with the report of ZUO et al [21].

Figure 3 displays the XRD patterns of the squeeze-cast Al−5.0Mg−3.0Zn−1.0Cu alloy. It is found that the squeeze-cast alloy is composed of

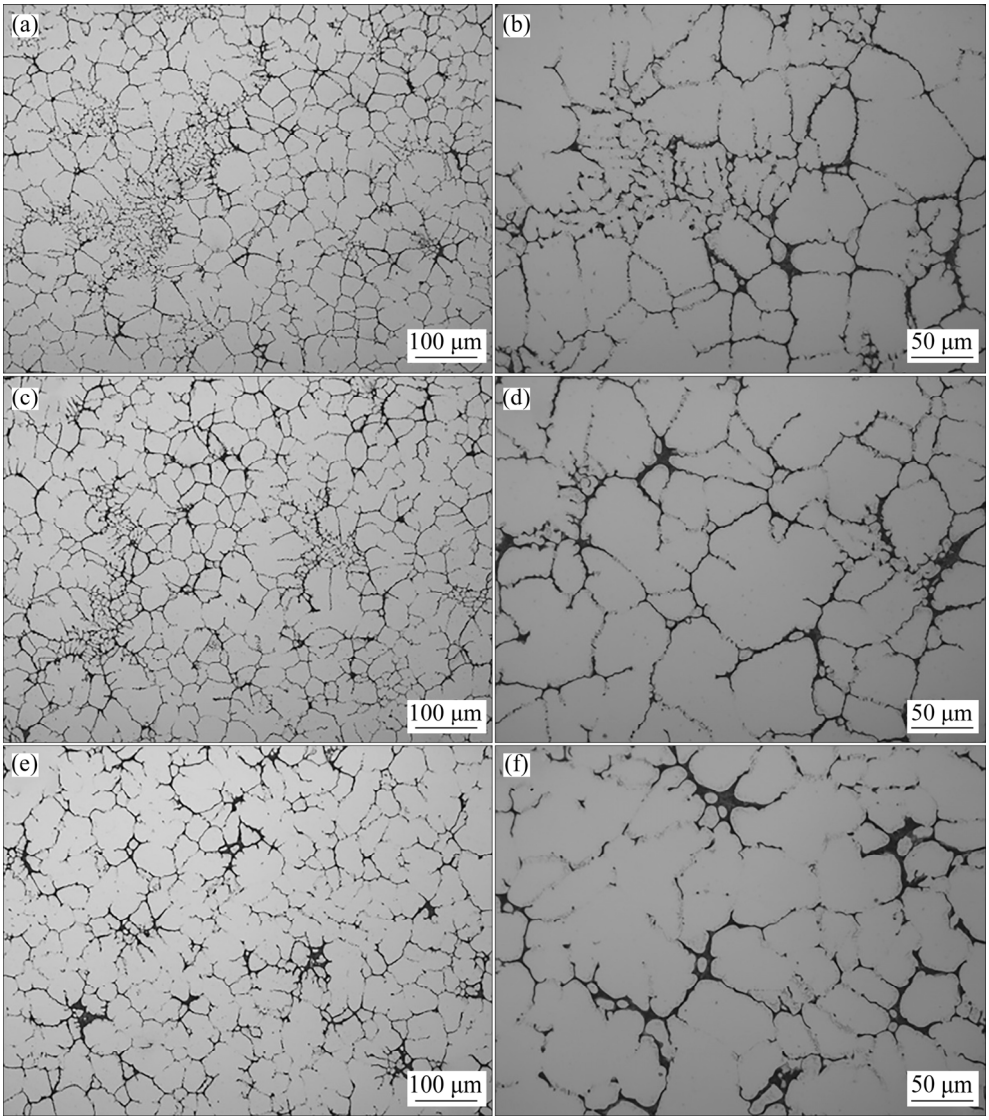

Fig. 2 Microstructures of squeeze-cast alloy at depths of 0 mm (a, b), 2.0 mm (c, d) and 4.0 mm (e, f)

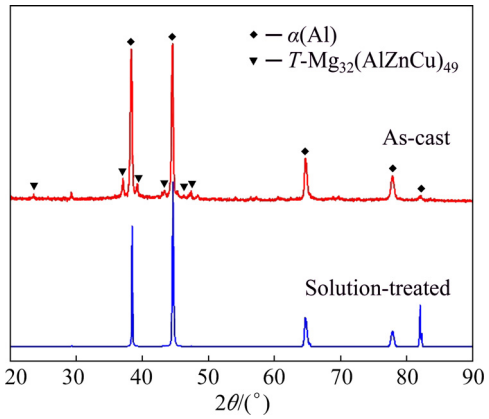

Fig. 3 XRD patterns of squeeze-cast alloy under different conditions

primary α(Al) and T-$Mg_{32}(AlZnCu)_{49}$ phase. In other words, the black strip-like secondary phase (Fig. 2) is the T phase according to the work of LI et al [22]. Meanwhile, the white and black phases are clearly observed in Fig. 4(a). The mapping scanning shows that the black phase mainly contains Al and little alloying elements of Mg, Zn and Cu, while the white phase involves higher amounts of the mentioned alloying elements. It seems that the black phase is the primary α(Al) phase in which little amounts of Mg, Zn, and Cu have been dissolved. Furthermore, scanning analysis of Point 1 indicates that the composition of the white phase is 69.8% Al, 20.7% Mg, 6.9% Zn,

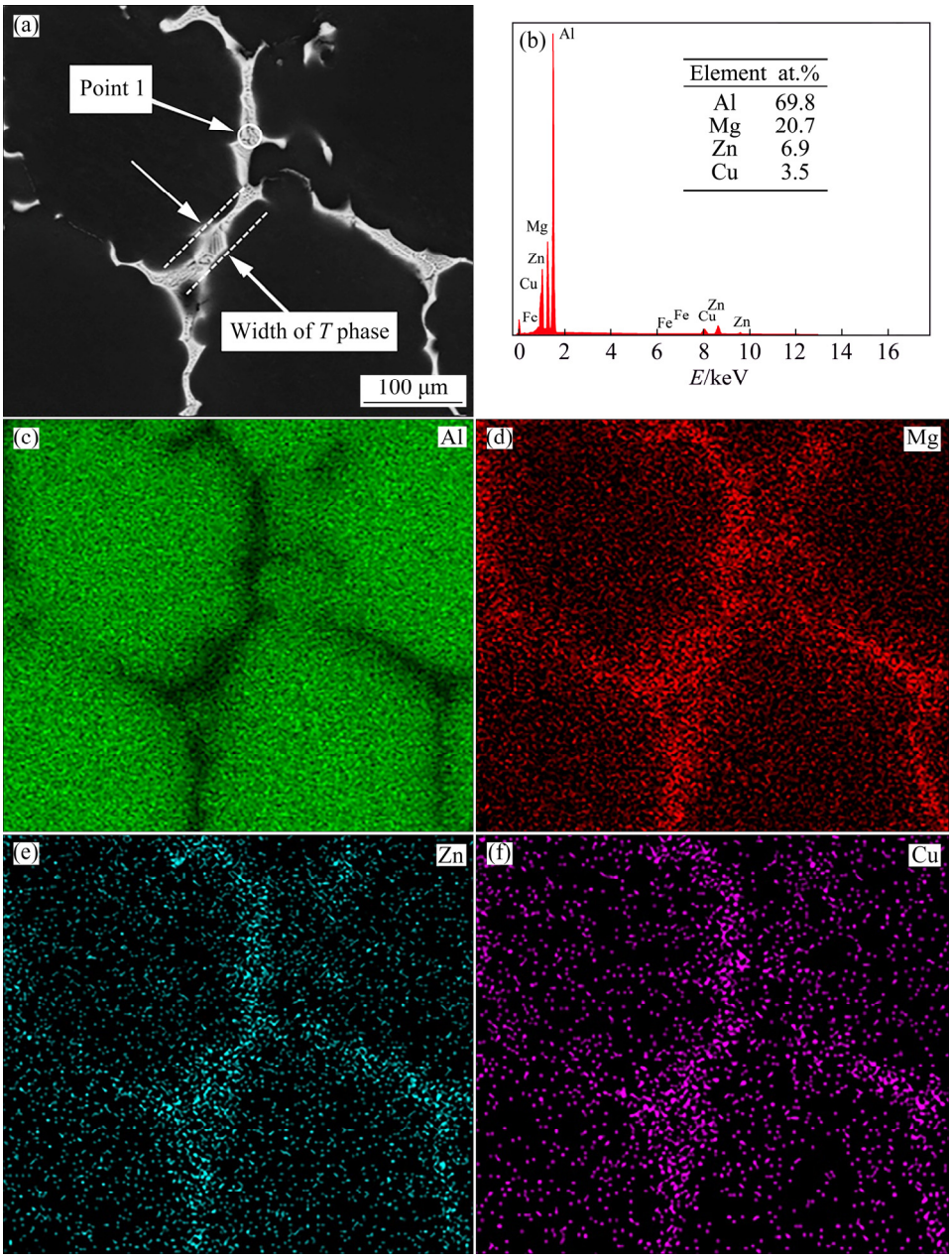

Fig. 4 Microstructures of squeeze-cast alloy: (a) SEM image; (b) EDS result of Point 1; (c−f) Related elemental maps

and 3.5% Cu (molar fraction). Thereby, it could be deduced that the studied alloy consists of primary α(Al) and T phases, which is in good consistency with the XRD results in Fig. 3.

Figure 5 shows the volume fraction, average width of the T phase, and the size of the primary α(Al) phase in the squeeze-cast alloy. In order to ensure the accuracy of the statistical analysis, at least 20 images were analyzed for each depth. By increasing the depth from 0 to 4 mm, the volume fraction of the T phase is reduced from 10.1% to 5.7%. By considering the reduction of cooling rate with the depth increment, the decrease of the T phase amount might be ascribed to the reduction of cooling rate. Meanwhile, the amount of the primary α(Al) phase is increased with the cooling rate reduction. Similar relationships between the cooling rate and the amount of primary α(Al) phase have also been reported in the Al−Fe−Si alloys [23]. Besides, the cooling rate affects the size of the eutectic T phase. As shown in Fig. 5, the average width of the T phase is increased from 1.9 to 5.1 μm with a cooling rate decreasing. From the analysis above, it can be noticed that the increased cooling rate not only refines the size but also increases the amounts of the T phase.

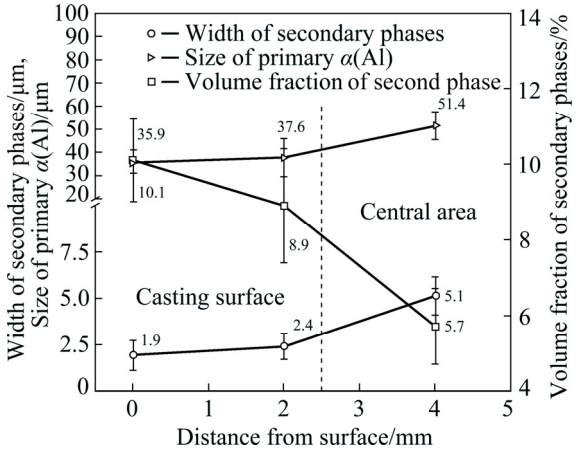

Fig. 5 Volume fraction, width of secondary phases, and size of primary α(Al) phase of squeeze-cast alloy with depth of specimen

As mentioned above, the cooling rate can affect both the size and amount of the T phase. In addition, it influences the size of the primary α(Al) phase. The average grain size of the primary α(Al) phase at different depths of the produced cast alloy is represented in Fig. 5. As the depth is increased from 0 to 4 mm, the average size of the primary α(Al) phase is increased from 35.9 to 51.4 μm. This indicates that the size of primary α(Al) decreases as the cooling rate increases due to the increment of the undercooling. The small size of the primary α(Al) grains stands for the fine microstructure formation and the uniform distribution of secondary phases in the matrix [24].

Tensile tests of the squeeze-cast alloy at different depths were performed and the results are listed in Table 2. By increasing the depth from 2.0 to 4.0 mm, both UTS and elongation decrease from 243.7 MPa and 2.3% to 217.9 MPa and 1.4%, respectively, while the yield strength (YS) does not change considerably. According to the microstructures in Figs. 2 and 5, the size and amount of the primary α(Al) and the distribution of the T phase are responsible for the mechanical properties of the squeeze-cast alloy. It can be summarized that a higher cooling rate not only refines the primary α(Al) and secondary T phases but also improves the amount of the T phase among the grain boundaries.

Table 2 Tensile properties of squeeze-cast alloy at different depths

Depth/mm	YS/MPa	UTS/MPa	Elongation/%
2.0	192.5±4.1	243.7±8.1	2.3±0.1
4.0	186.6±7.4	217.9±1.3	1.4±0.2

3.2 Microstructure and mechanical properties after solution treatment

Solution treatment was employed in order to dissolve the secondary T phase into the matrix. Also, proper solution temperature is critical during the solution treatment since a higher solution temperature can lead to the overburning, which undermines the mechanical properties of alloys. It was reported that 470 °C is a suitable temperature for Al−Zn−Mg−Cu alloys [25,26] and previous study [19] has demonstrated that most of the secondary phases in Al−5.0Mg−3.0Zn−1.0Cu can be dissolved into the matrix at 470 °C for 24 h. So, the solution treatment temperature was chosen at 470 °C.

Figures 6 and 7 show the optical micrographs of the squeeze-cast alloy after the solution treatment at 470 °C for different time. It should be mentioned that the samples used for observation were cut from the depth of 2.0 and 4.0 mm. As can be seen, the evolutions of morphology and content of secondary

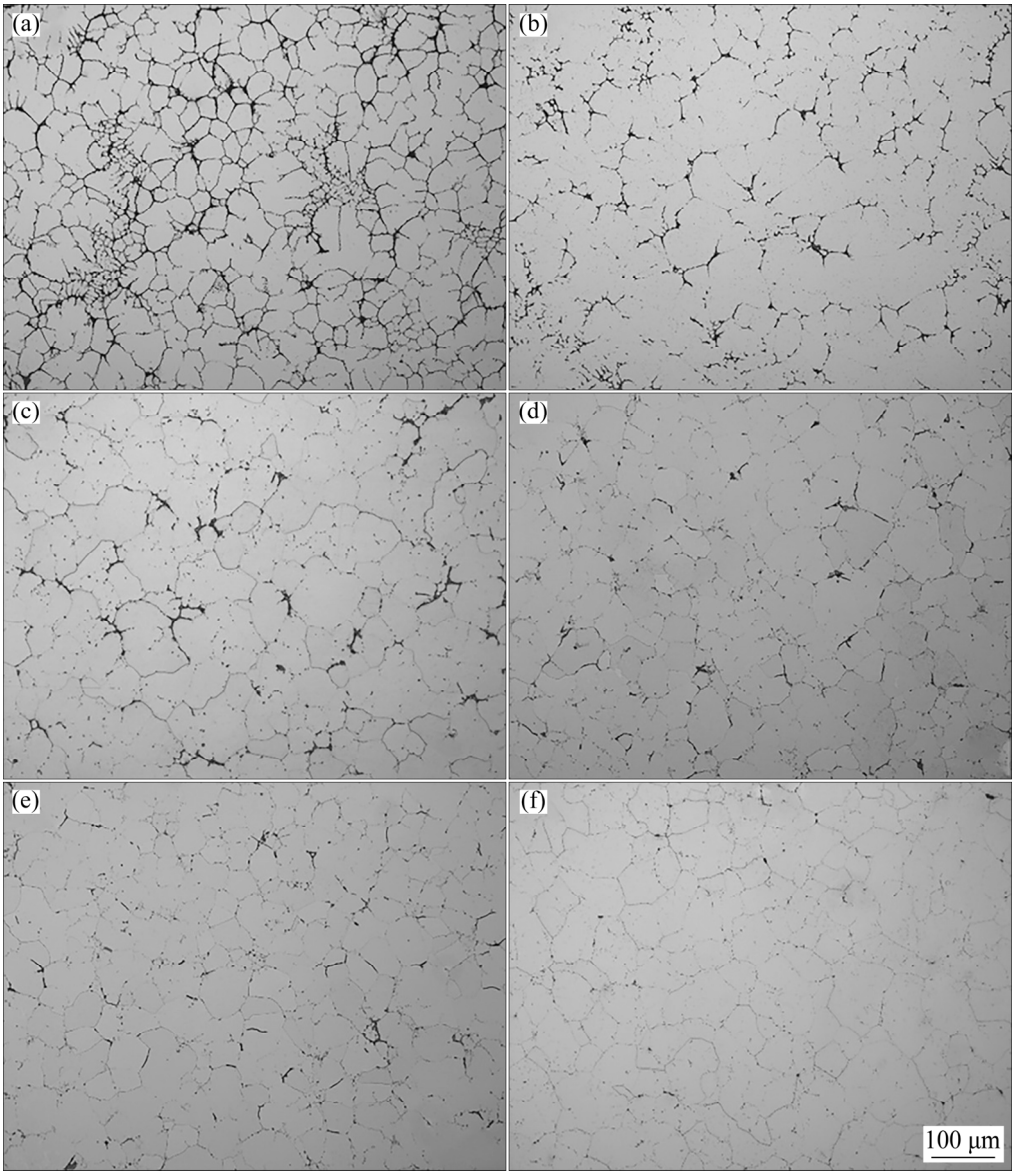

Fig. 6 Microstructures of Al−5.0Mg−3.0Zn−1.0Cu alloy at depth of 2.0 mm in different states: (a) Squeeze-cast; (b−f) Solution treated at 470 °C for 1 h (b), 4 h (c), 12 h (d), 24 h (e) and 36 h (f)

phases are highly dependent on the solution-treated time. After solution treatment at 470 °C for 4 h, the discontinuous secondary phases are clearly recognized (Fig. 6(c) and Fig. 7(c)), while the secondary phases disappear after being solution-treated at 470 °C for 36 h (Figs. 6(f) and 7(f)). Figure 8 exhibits the volume fraction of the secondary phases at 470 °C for different solution time. As the solution time is increased from 0 to 36 h, the volume fraction of the *T* phase at the depth of 2.0 mm is reduced from 8.9% to 0.2%, and the volume fraction at the depth of 4.0 mm is decreased from 5.7% to 0.3%. The average grain size also changes considerably during the solution treatment. After the solution treatment for 36 h, the *T* phase is dissolved into the matrix. At the depth of 2.0 mm, the average grain size is increased to 50.1 μm and at depth of 4.0 mm, the average grain grows to 84.2 μm. So, as the solution time increases up to 470 °C, the grain size tends to coarsen. To avoid further coarsening of grains, the optimum solution treatment of the studied alloy is chosen to be 470 °C, 36 h.

The tensile properties of the solution-treated alloys at the depth of 2.0 and 4.0 mm are listed in Table 3. In general, the mechanical properties are improved dramatically after the solution treatment. At the depth of 2.0 mm, YS and UTS are increased

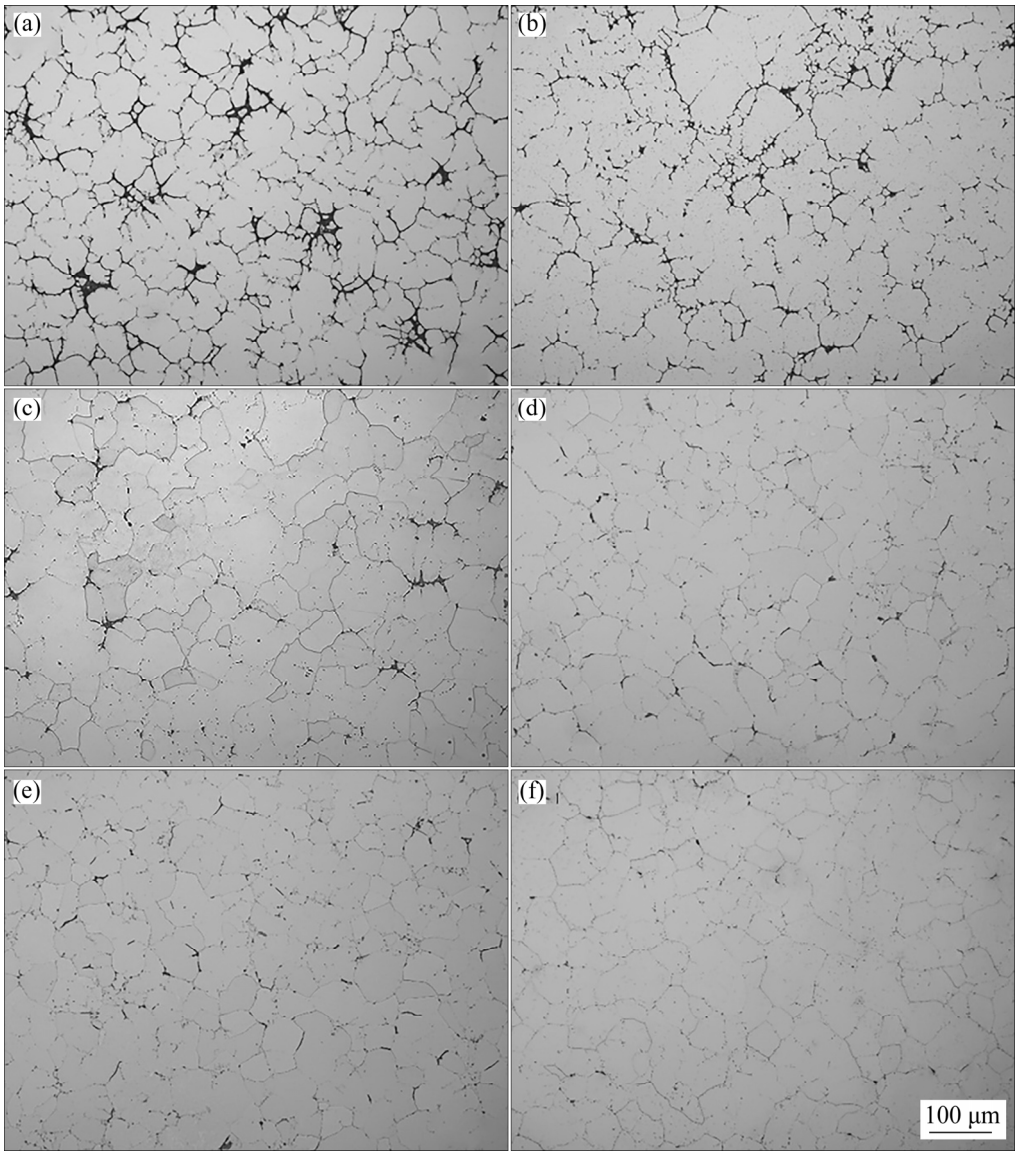

Fig. 7 Microstructures of Al−5.0Mg−3.0Zn−1.0Cu alloy at depth of 4.0 mm in different states: (a) Squeeze-cast; (b−f) Solution treated at 470 °C for 1 h (b), 4 h (c), 12 h (d), 24 h (e) and 36 h (f)

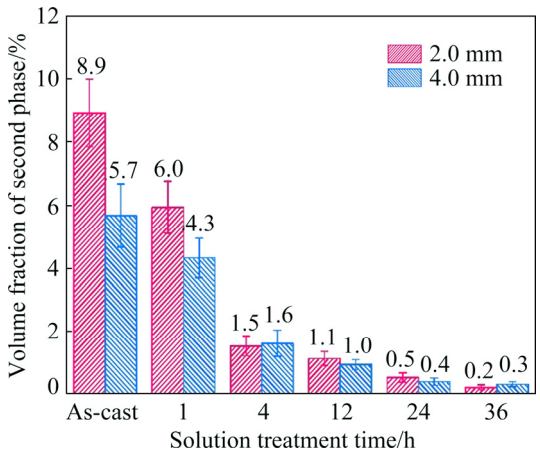

Fig. 8 Volume fraction of *T* phase at depth of 2.0 and 4.0 mm after solution treatment at 470 °C for different time

Table 3 Tensile properties of solution-treated alloy at depths of 2.0 and 4.0 mm

Depth/mm	YS/MPa	UTS/MPa	Elongation/%
2.0	232.6±11.9	387.8±1.5	18.6±0.7
4.0	226.8±1.5	348.9±10.3	13.9±1.6

respectively to 232.6 and 387.8 MPa. The elongation to failure of the squeeze-cast alloy is only 2.3%, while that of the solution-treated alloy is notably improved to 18.6%. At the depth of 4.0 mm, both YS and UTS increase to 226.8 and 348.9 MPa. The elongation to failure of the squeeze-cast alloy is only 1.4%, while that of the solution-treated alloy is significantly enhanced to 13.9%.

There are two main reasons for the improvement of the mechanical properties after the solution treatment including the dissolution of the secondary phases and the solid solution strengthening effect. On one hand, due to the decrease in the volume fraction of the secondary phase among the grain boundaries, the stress concentration is relieved. Therefore, it is easier for dislocations to move from one grain to another instead of forming dislocation pile-ups against the grain boundaries. Consequently, the ductility of the alloy at the depths of 2.0 and 4.0 mm is increased notably from to 18.6% and 13.9%, respectively, after solution treatment. Moreover, as the alloying elements are dissolved into the matrix in the solution-treated alloy, the solid solution strengthening occurs. This effect not only resolves the weakening of the secondary phases on the ductility but also further increases the strength of the alloy. As a result, both YS and the UTS of the solution treated specimen are significantly improved. It should be noted that the strength at the depth of 2.0 mm is higher than that at the depth of 4.0 mm. As shown in Fig. 8, the volume fraction of the secondary phases at the depth of 2.0 mm is also higher than that at the depth of 4.0 mm. This means that more alloying elements are dissolved into the matrix for the alloy at the depth of 2.0 mm after the solution treatment. Hence, a higher solid solution strengthening effect is obtained leading to the alloy with higher strength.

As presented in Fig. 9, the fracture morphologies have obvious differences between the squeeze-cast and solution-treated alloys. For the squeeze-cast alloy, a river-like fracture pattern and some cleavage traces can be found in Figs. 9(a, c), while the fracture surface of the solution-treated alloy is characterized by the ductile inter-granular fracture according to Figs. 9(b, d). In this regard, different fracture morphologies are related to the content of secondary phases in the microstructure. For the squeeze-cast alloy, these brittle secondary phases along the grain boundaries cause a brittle fracture. After the solution treatment, most of the secondary phases are dissolved into the matrix. During the tensile test, stress concentration is reduced and deformation becomes more uniform. As a result, ductile fracture occurs, which is consistent with the improved ductility observed in the solution-treated alloy.

3.3 Microstructure and mechanical properties after aging treatment

Figures 10(a, b) show the microstructures of

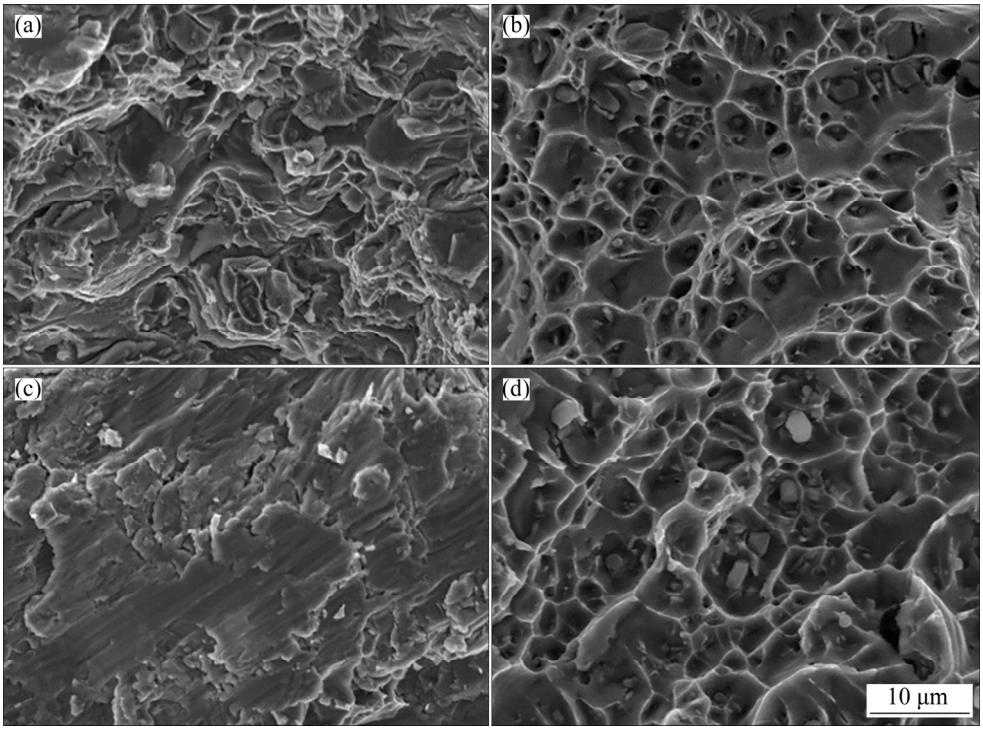

Fig. 9 Fracture morphologies of Al−5.0Mg−3.0Zn−1.0Cu alloy at depth of 2.0 mm (a, b) and 4.0 mm (c, d): (a, c) Squeeze-cast; (b, d) Solution treated at 470 °C for 36 h

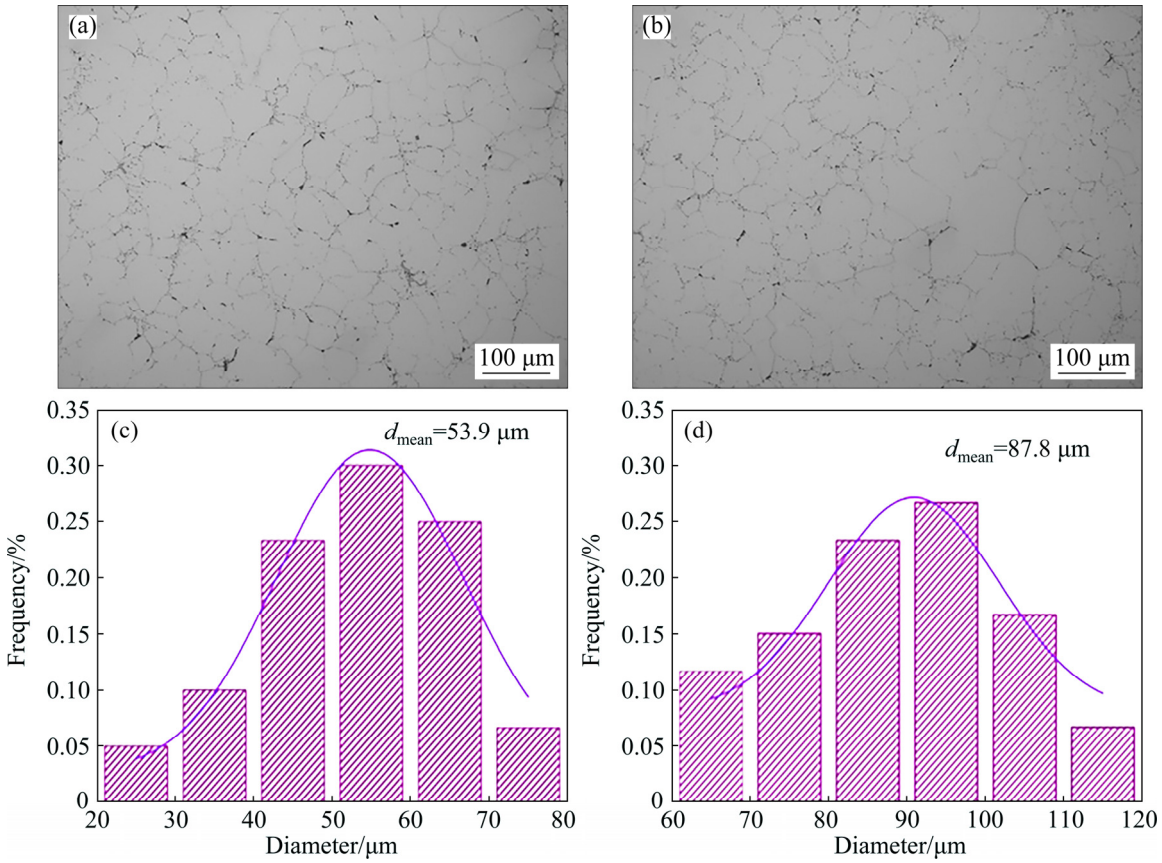

Fig. 10 Microstructures (a, b) and corresponding grain size distribution of α(Al) grains (c, d) of peak-aged alloy at different depths: (a, c) 2.0 mm, (b, d) 4.0 mm

the alloy after the aging treatment. Clearly, the grain size at the depth of 2.0 mm is smaller than that at the depth of 4.0 mm. The grain size distribution of α(Al) grains at different positions is shown in Figs. 10(c, d). It can be seen that the grain size is increased from 53.9 to 87.8 μm with the depth increasing from 2.0 to 4.0 mm.

Aging treatment at 120 °C was performed on the solution-treated alloy in order to further improve the strength of the material. The aging-hardening curves of the investigated alloy at the depths of 2.0 and 4.0 mm are shown in Fig. 11. Both hardening curves increase markedly during the first 4 h, reaching the peak at 24 h, and then slightly decrease after the peak-aging. This phenomenon is related to the decomposition of the supersaturated solid solution and the formation of precipitates. The peak aging is attained at 120 °C for 24 h, similar to the peak aging condition of Al−Zn−Mg−Cu alloy in the previous study [27].

The tensile properties of the peak-aged alloy at different depths are listed in Table 4. The average tensile strength of 449.5 MPa and elongation to

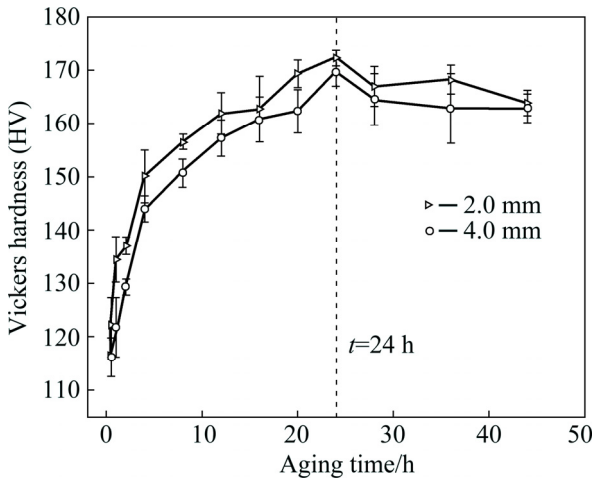

Fig. 11 Aging-hardening curves of Al−5.0Mg−3.0Zn−1.0Cu alloy at depths of 2.0 and 4.0 mm aged at 120 °C

Table 4 Tensile properties of peak-aged alloy at two different depths of 2.0 and 4.0 mm

Depth/mm	YS/MPa	UTS/MPa	Elongation/%
2.0	345.1±12.7	449.5±8.6	12.5±1.7
4.0	329.1±3.4	421.4±5.8	8.1±0.5

failure of 12.5% are obtained for the depth of 2.0 mm, while the average tensile strength of 421.4 MPa and elongation of 8.1% are measured at the of depth 4.0 mm. These results indicate that the squeeze-cast alloy could possess a suitable combination of tensile strength and ductility. However, the ductility at 4.0 mm is much lower than that at the depth of 2.0 mm.

The fracture morphologies of the peak-aged alloy at the depths of 2.0 and 4.0 mm are exhibited in Fig. 12. It can be seen that all fracture surfaces show ductile fracture characteristics. As represented in Figs. 12(c, d), many dimples are clearly observed at the depth of 4.0 mm. However, the size and the depth of these dimples are not as large as those at the depth of 2.0 mm according to Figs. 12(a, b), indicating a decrease in ductility. Therefore, the ductility from the depth of 2.0 to 4.0 mm decreases from 12.5% to 8.1%.

Figure 13(a, c) represent the bright-field (BF) TEM micrographs in the $\langle 112\rangle_{Al}$ orientation of the peak-aged alloy at the depths of 2.0 and 4.0 mm, respectively. As shown, the precipitates have no distinct differences along the depth, and elliptical precipitates can be found along the $\langle 112\rangle_{Al}$ orientation. Also, Figs. 13(b, d) show the selected area electron diffraction (SAED) patterns in $\langle 112\rangle_{Al}$ zone axes of the alloy at different depths. According to the previous study [28−31], precipitation sequence of Al−Zn−Mg−Cu alloy is as follows: supersaturated solid solution (SSS) → coherent G.P. zone → η' phase (semi-coherent precipitate) → η phase (stable precipitate). The SAED patterns indicate that there exist the diffraction spots of η' phase and G.P. II zone in which the intensity of η' phase is larger than that of the G.P. II zone. This means that the η' phase is the major precipitate of the peak-aged alloy [32]. However, a small amount of the G.P. II zone also has significant effects on the strengthening effect. On one hand, numerous η' precipitate can block the dislocation motion. This is the reason for the enhanced mechanical properties of the peak-aged alloy. Furthermore, the existence of the G.P. II zone in the α(Al) matrix can mitigate the hindrance of η' phase, since G.P. II zone is coherent with α(Al) matrix while the η' phase is semi-coherent with the α(Al) matrix. Consequently, a good combination of strength and ductility is obtained. From the above analysis, similar morphology and distribution of precipitates at different depths under the peak-aging condition indicate that different mechanical properties observed at various depths might be attributed to their grain size according to the Hall−Petch relationship.

It is generally accepted that the grain size

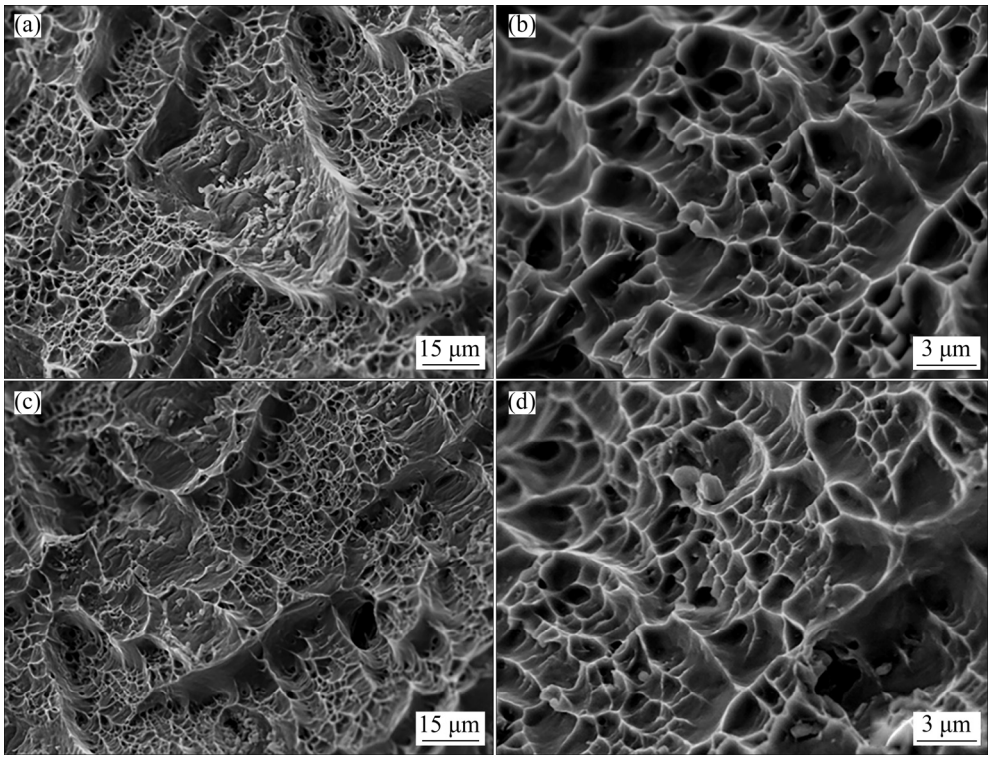

Fig. 12 Fracture morphologies of peak-aged alloy at different depths: (a, b) 2.0 mm; (c, d) 4.0 mm

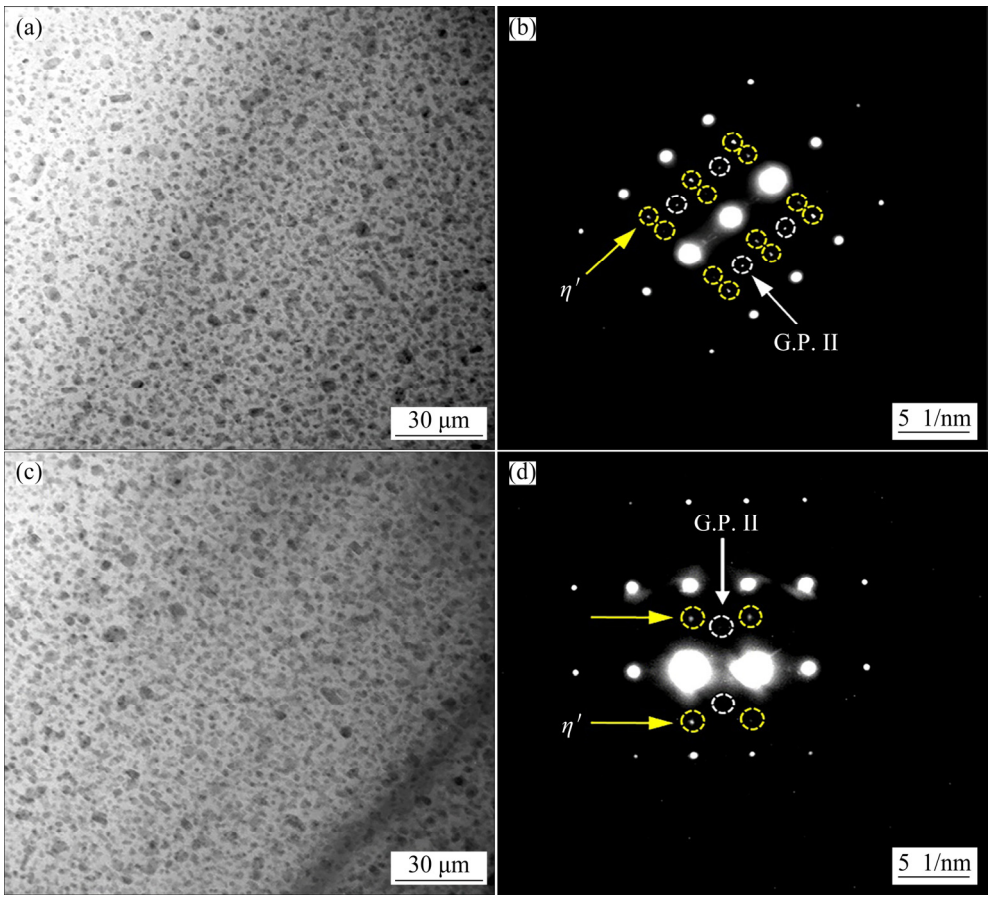

Fig. 13 Bright-field TEM images of precipitates viewed along $\langle 112\rangle_{Al}$ zone axis (a, c) and corresponding selected area electron diffraction patterns (b, d) of peak-aged alloy at different depths: (a, b) 2.0 mm; (c, d) 4.0 mm

plays an important role in determining the mechanical properties of metals and alloys. Small grain size has a high density of grain boundary which can efficiently block the movement of dislocations, giving a higher strength. Also, a small grain size indicates a fine and uniform structure. The internal stress during the deformation can uniformly distribute in all grains, which increases the ductility. Consequently, the alloy at the depth of 2.0 mm possesses better mechanical properties than that at the depth 4.0 mm.

4 Conclusions

(1) For the squeeze-cast alloy, the micro-structure consists of equiaxed α(Al) and secondary T-$Mg_{32}(AlZnCu)_{49}$ phase. As the depth increases from 0 to 4.0 mm, both grain size and the width of the T phase increase; however, the volume fraction of the T phase drops. Consequently, the related UTS and elongation reduce from 243.7 MPa and 2.3% to 217.9 MPa and 1.4%, respectively.

(2) For solution-treated alloy, most of the T phase is dissolved into the matrix after solution-treatment at 470 °C for 36 h, resulting in a remarkable increase in strength and ductility. As the depth increases from 2.0 to 4.0 mm, the grain size increases from 50.1 to 84.2 μm. So, the UTS and elongation reduce from 387.8 MPa and 18.6% to 348.9 MPa and 13.9%, respectively.

(3) The precipitation process strongly affects the hardness and strength during the aging-treatment. After the peak-aging at 120 °C for 24 h, precipitates of the alloy are G.P. II zone and metastable η' phase. From the depth of 2.0 to 4.0 mm, the YS, UTS and elongation decrease from 345.1 MPa, 449.5 MPa and 12.5% to 329.1 MPa, 421.4 MPa and 8.1%, respectively. Additionally, the different strengths along the depth are related to the increased grain size from 53.9 to 87.8 μm.

References

[1] ZHAO Pi-zhi, TSUCHIDA T. Effect of fabrication

conditions and Cr, Zr contents on the grain structure of 7075 and 6061 aluminum alloys [J]. Materials Science and Engineering A, 2009, 499: 78−82.

[2] LIU Dan, ATKINSON H V, KAPRANOS P, JIRATTITICHAROEAN W, JONES H. Microstructural evolution and tensile mechanical properties of thixoformed high performance aluminium alloys [J]. Materials Science and Engineering A, 2003, 361: 213−224.

[3] KIM W Y, KANG C G, KIM B M. Deformation behavior of wrought aluminum alloys in incremental compression experiment with a closed die [J]. Journal of Materials Processing Technology, 2007, 191: 372−376.

[4] EBRAHIMI S H S, EMAMY M. Effects of Al−5Ti−1B and Al−5Zr master alloys on the structure, hardness and tensile properties of a highly alloyed aluminum alloy [J]. Materials & Design, 2010, 31: 200−209.

[5] GOVINDARAJU H K, JAYARAJ T, SADANANDARAO P R, VENKATESHA C S. Evaluation of mechanical properties of as-cast Al−Zn−Ce alloy [J]. Materials & Design, 2010, 31(S): s24−s29.

[6] FAN Cai-he, CHEN Zhen-hua, HE Wu-qiang, CHEN Jiang-hua, CHEN Ding. Effects of the casting temperature on microstructure and mechanical properties of the squeeze-cast Al−Zn−Mg−Cu alloy [J]. Journal of Alloys and Compounds, 2010, 504: L42−L45.

[7] SAIKAWA S, AOSHIMA G, IKENO S, MORITA K, SUNAYAMA N, KOMAI K. Microstructure and mechanical properties of an Al−Zn−Mg−Cu alloy produced by gravity casting process [J]. Archives of Metallurgy and Materials, 2015, 60: 871−874.

[8] GAO Tong, ZHANG Yong-rui, LIU Xiang-fa. Influence of trace Ti on the microstructure, age hardening behavior and mechanical properties of an Al−Zn−Mg−Cu−Zr alloy [J]. Materials Science and Engineering A, 2014, 598: 293−298.

[9] YANG Guang-yu, MENG Hong-shuai, LIU Shao-jun, QI Yuan-hao, JIE Wan-qi. Microstructures and room temperature mechanical properties of Al−6.3Zn−2.8Mg−1.8Cu casting aluminum alloy [J]. Acta Metall Sin, 2012, 48: 211−219.

[10] GALLERNEAULT M, DURRANT G, CANTOR B. Eutectic channelling in a squeeze cast Al−4.5Wt%Cu alloy [J]. Scripta Metallurgica et Materialia, 1995, 32: 1553−1557.

[11] LI Xin-we, CAI Qi-zhou, ZHAO Bing-yi, XIAO Ya-ting, LI Bin. Effect of nano TiN/Ti refiner addition content on the microstructure and properties of as-cast Al−Zn−Mg−Cu alloy [J]. Journal of Alloys and Compounds, 2016, 675: 201−210.

[12] HAN Zhi-qiang, HUANG Xiao-ran, LUO A A, SACHDEVB A K, LIU Bai-cheng. A quantitative model for describing crystal nucleation in pressurized solidification during squeeze casting [J]. Scripta Materialia, 2012, 66: 215−218.

[13] GHOMASHCHI M R, VIKHROV A. Squeeze casting: An overview [J]. Journal of Materials Processing Technology, 2000, 101: 1−9.

[14] SHEHATA F. Squeeze casting of Al−Cu and Al−Si alloys [J]. Advanced Materials and Processes, 1994, 4: 136−140.

[15] HASHEMI H R, ASHOORI H, DAVAMI P. Microstructure and tensile properties of squeeze cast Al−Zn−Mg−Cu alloy [J]. Materials Science and Technology, 2001, 17: 639−644.

[16] CHADWICK G A, YUE T M. Principles and applications of squeeze casting [J]. Metals and Materials, 1989, 5: 6−12.

[17] YUE T M, CHADWICK G A. Squeeze casting of light alloys and their composites [J]. Journal of Materials Processing Technology, 1996, 58: 302−307.

[18] CHOI S W, KIM Y M, LEE K M, CHOB H S, HONGB S K, KIMA Y C, KANGA C S, KUMAI S. The effects of cooling rate and heat treatment on mechanical and thermal characteristics of Al−Si−Cu−Mg foundry alloys [J]. Journal of Alloys and Compounds, 2014, 617: 654−659.

[19] TANG Hua-ping, WANG Qu-dong, LEI Chuan, YE Bing, WANG Kui, JIANG Hai-yan, DING Wen-jiang, ZHANG Xiang-feng, LIN Zhen, ZHANG Ji-bin. Effect of cooling rate on microstructure and mechanical properties of an Al−5.0Mg−3.0Zn−1.0Cu cast alloy [J]. Journal of Alloys and Compounds, 2019, 801: 596−608.

[20] POURKIA N, EMAMY M, FARHANGI H, SEYED EBRAHIMI S H. The effect of Ti and Zr elements and cooling rate on the microstructure and tensile properties of a new developed super high-strength aluminum alloy [J]. Materials Science and Engineering A, 2010, 527: 5318−5325.

[21] ZUO Yo-bo, CUI Jian-zhong, ZHAO Zhi-hao, ZHANG Hai-tao, LI Lei, ZHU Qing-feng. Mechanism of grain refinement of an Al−Zn−Mg−Cu alloy prepared by low-frequency electromagnetic casting [J]. Journal of Materials Science, 2012, 47: 5501−5508.

[22] LI Bo, PAN Qing-lin, CHEN Cong-ping, WU Hai-hua, YIN Zhi-min. Effects of solution treatment on microstructural and mechanical properties of Al−Zn−Mg alloy by microalloying with Sc and Zr [J]. Journal of Alloys and Compounds, 2016, 664: 553−564.

[23] DUTTA B, RETTENMAYR M. Effect of cooling rate on the solidification behaviour of Al−Fe−Si alloys [J]. Materials Science and Engineering A, 2000, 283: 218−224.

[24] OKAYASU M, TAKASU S, MIZUNO M. Relevance of instrumented nano-indentation for the assessment of the mechanical properties of eutectic crystals and α(Al) grain in cast aluminum alloys [J]. Journal of Materials Science, 2012, 47: 241−250.

[25] WANG Fei-fan, MENG Wen, ZHANG Hong-wei, HAN Zhi-qiang. Effects of under-aging treatment on microstructure and mechanical properties of squeeze-cast Al−Zn−Mg−Cu alloy [J]. Transactions of Nonferrous Metals Society of China, 2018, 28: 1920−1927.

[26] LI Xin-wei, CAI Qi-zhou, ZHAO Bing-yi, LIU Bo, LI Wen-wu. Precipitation behaviors and properties of solution-aging Al−Zn−Mg−Cu alloy refined with TiN nanoparticles [J]. Journal of Alloys and Compounds, 2018, 746: 462−470.

[27] KIM S W, KIM D Y, KIM W G, WOO K D. The study on characteristics of heat treatment of the direct squeeze cast 7075 wrought Al alloy [J]. Materials Science and Engineering A, 2001, 304: 721−726.

[28] LI Hong-ying, LIU Jiao-jiao, YU Wei-chen, ZHAO Hui, LI De-wang. Microstructure evolution of Al−Zn−Mg−Cu alloy during non-linear cooling process [J]. Transactions of Nonferrous Metals Society of China, 2016, 26: 1191−1200.

[29] ZHANG Yu-ha, YANG Shu-cai, JI Hong-zhi. Microstructure evolution in cooling process of Al−Zn−Mg−Cu alloy and kinetics description [J]. Transactions of Nonferrous Metals Society of China, 2012, 22: 2087−2091.

[30] KANG Lei, ZHAO Gang, WANG Guang-dong, LIU Kun, TIAN Ni. Effect of different quenching processes following solid-solution treatment on properties and precipitation behaviors of 7050 alloy [J]. Transactions of Nonferrous Metals Society of China, 2019, 29: 2162−2172.

[31] KHALFALLAH A, RAHO A A, AMZERT S, DJEMLI A. Precipitation kinetics of GP zones, metastable η' phase and equilibrium η phase in Al−5.46wt.%Zn−1.67wt.%Mg alloy [J]. Transactions of Nonferrous Metals Society of China, 2019, 29: 233−241.

[32] LI Yi-yun, KOVARIK L, PHILLIPS P J, HSU Y F, WANG W H, MILLS M J. High-resolution characterization of the precipitation behavior of an Al−Zn−Mg−Cu alloy [J]. Philosophical Magazine Letters, 2012, 92: 166−178.

固溶态和时效态挤压铸造 Al−5.0Mg−3.0Zn−1.0Cu 合金的显微组织及力学性能

刘天文，王渠东，汤华平，李仲洋，雷 川，Mahmoud EBRAHIMI，蒋海燕，丁文江

上海交通大学 材料科学与工程学院，
轻合金精密成型国家工程研究中心和金属基复合材料国家重点实验室，上海 200240

摘 要：研究 Al−5.0Mg−3.0Zn−1.0Cu 合金挤压铸造态、固溶态和时效态显微组织及力学性能随截面深度的变化规律。对于挤压铸造态合金，从表层到心部，α(Al)的晶粒尺寸和 T-$Mg_{32}(AlZnCu)_{49}$ 相的宽度显著增加，而 T-$Mg_{32}(AlZnCu)_{49}$ 相的体积分数显著下降，这些变化导致挤压铸造态合金抗拉强度从 243.7 MPa 降低到 217.9 MPa，伸长率从 2.3%降低到 1.4%。在 470 °C 下固溶处理 36 h 后，大部分第二相溶解于 α(Al)基体中，并且表面和心部的晶粒尺寸均较挤压铸造态的增大，从表层到心部，合金的伸长率从 18.6%降低到 13.9%，抗拉强度从 387.8 MPa 降低到 348.9 MPa。在 120 °C 下进一步时效 24 h 后，在基体中析出 G.P. II 区和 η'相，合金表层和心部的抗拉强度分别增加到 449.5 MPa 和 421.4 MPa，而伸长率则降至 12.5%和 8.1%。

关键词：挤压铸造 Al−Zn−Mg−Cu 合金；固溶处理；时效；显微组织；力学性能

(Edited by Bing YANG)